Composites: Part B 60 (2014) 359–370

Contents lists available at ScienceDirect

Composites: Part B

journal homepage: www.elsevier.com/locate/compositesb

Influence of matrix flowability, fiber mixing procedure, and curing conditions on the mechanical performance of HTPP-ECC

Burak Felekoglu [a], Kamile Tosun-Felekoglu [a,*], Ravi Ranade [b], Qian Zhang [b], Victor C. Li [b]

[a] Department of Civil Eng., Dokuz Eylul University, Izmir, Turkey
[b] Department of Civil and Environmental Eng., University of Michigan, Ann Arbor, MI, USA

ARTICLE INFO

Article history:
Received 8 October 2013
Received in revised form 10 December 2013
Accepted 27 December 2013
Available online 6 January 2014

Keywords:
A. Fibers
B. Mechanical properties
E. Cure
Engineered Cementitious Composites

ABSTRACT

In this study, the influences of matrix flowability, fiber mixing procedure, and curing conditions on the mechanical properties of Engineered Cementitious Composites (ECC) made with High Tenacity Polypropylene (HTPP) fibers are investigated. While the HTPP-ECC examined in this study possesses moderate compressive strengths (30–70 MPa), their tensile ductility (1.91–3.91%) is similar to that of ECC with Polyvinyl Alcohol (PVA) fibers. For the purpose of controlling matrix flowability, different dosages of HRWR admixture were introduced to a matrix with fly ash/cement weight ratio of 2.8 and water/cementitious material weight ratio of 0.23. Dogbone-shaped and 50 mm cube specimens were used to investigate uniaxial tensile and compressive properties of HTPP-ECC, respectively. Test results showed that control of flowability in a certain range is required to achieve robust tensile ductility. A further improvement in tensile ductility and mechanical properties of HTPP-ECC was achieved through water-curing instead of air curing typically used for PVA-ECC. The basic mechanisms that enhance tensile ductility of HTPP-ECC through flowability control, mixing procedure modification, and water-curing are discussed from the view point of micromechanics underlying ECC design, with supporting evidence from fiber bridging stress–crack width (σ–δ) relations.

© 2014 Elsevier Ltd. All rights reserved.

1. Introduction

Over the last two decades, Engineered Cementitious Composites (ECC) have been developed to address the shortcoming of brittleness in conventional plain concrete. Unlike plain concrete and normal fiber reinforced concrete (FRC), ECC shows a tensile strain hardening behavior after first cracking and develops a high tensile ductility in the range of 3–7% [1], while conventional concrete fractures only at about 0.01% tensile strain with a localized crack of infinite width [2,3]. Due to this reason, successfully tailored ECC is also referred as strain hardening cementitious composites (SHCC) [4]. Tensile ductility of ECC is engineered through a micromechanics-based design framework developed by Li [5] which is summarized in Section 4. In contrast to the design of ultra high strength concrete, ECC benefits from the pre-existing flaws by managing their size range rather than by eliminating them. Typically, the damage pattern under uniaxial tension is a large number of closely spaced microcracks of widths less than 100 μm, spaced a few millimeters apart. During multiple microcrack development, the tensile load continues to increase. In this manner, localized catastrophic brittle fracture is suppressed, in favor of strain-hardening. The ductility of ECC is the sum total of distributed deformation resulting from the diffused microcrack damage until the tensile capacity of bridging fibers on one of these microcracks is exhausted [6].

Using the micromechanics-based conditions for multiple cracking and the pseudo strain-hardening (PSH) indices described in Section 4.1, ECC with various fiber types have been designed. The first ECC reported in literature with significant strain-hardening behavior was prepared with polyethylene (PE) Spectra® fiber. The interface of PE fibers with the matrix was tailored using plasma treatment to enhance the fiber/matrix bond [5,7]. However, the PE fiber is very expensive and alternative polymer fibers, particularly Polyvinyl Alcohol (PVA), were explored for producing ECC [8–10]. PVA fiber, unlike the PE fiber, forms a strong chemical bond with the cementitious matrix, in addition to frictional bond. As a result, instead of plasma treatment used for PE fibers to increase the fiber/matrix bond, an oil coating is applied on the PVA fibers to reduce the fiber/matrix bond that may otherwise rupture the fiber during pullout. Such interface tailoring ensures synergistic interaction between fiber, matrix, and interface, which is the key for achieving high tensile ductility [11].

Even though the PVA fibers are cheaper than PE fibers, they still account for approximately 50% of the total material cost of ECC. Recycled plastic fibers and hybrid fiber reinforcement may also be employed as cost effective fibers in ECC design, if fiber, matrix

* Corresponding author. Tel.: +90 232 3017059; fax: +90 232 3017253.
E-mail address: kamile.tosun@deu.edu.tr (K. Tosun-Felekoglu).

1359-8368/$ - see front matter © 2014 Elsevier Ltd. All rights reserved.
http://dx.doi.org/10.1016/j.compositesb.2013.12.076

and interface properties are modified according to micromechanical theory proposed by Li [4]. There are many studies regarding the utilization of recycled plastic fibers in concrete for the purpose of ductility improvement and cracking control [12–15]. However, most of these studies reported tension and/or deflection softening behavior at low fiber dosages (<2% by volume) mostly due to the incompatible matrix-interface properties to provide robust multiple cracking behavior. There is no doubt that steel fibers significantly improve the ductility, post cracking strength and crack opening behavior of plain concrete up to a certain dosage (usually between 20 and 80 kg/m^3 for workability reason) [16,17]. However, this dosage range is not enough to provide multiple cracking and strain hardening behavior if a sufficient physical modification on steel fibers' geometry (such as twisting) is not performed [18].

In order to further decrease the cost of ECC, High Tenacity Polypropylene (HTPP) fibers have been studied in the past as alternatives to other fibers by Yang [3]. Recently, HTPP fibers with tensile strength of 800–900 MPa and diameters of 10–12 μm diameter are commercially available. Yang [3] developed HTPP-ECC incorporating 2% HTPP fiber (by total mix volume) using the micromechanics-based design approach, which exhibited tensile strain capacity as high as 4% with 2–2.5 MPa ultimate tensile strength.

A major drawback of HTPP-ECC is its difficult processing due to very high aspect ratio of HTPP fibers. Micromechanical analysis suggests that a high aspect ratio (length/diameter ratio) is needed for fibers, such as HTPP, with low interfacial bond with the matrix to effectively bridge the micro-cracks in ECC. However, due to their high aspect ratio, HTPP fibers are susceptible to clumping and poor dispersion in a cementitious matrix. At equivalent fiber dosage (2%) the number of HTPP fibers (12 μm diameter, 10 mm length) per cubic meter of ECC is nearly 12.7 times higher than that of PVA fibers (39 μm diameter, 12 mm length) in PVA-ECC. Due to this reason, proper mixing of HTPP fibers in a cementitious matrix even at comparatively low fiber dosages is a challenging task.

The objective of this study is to enhance the magnitude and consistency of the composite mechanical properties of HTPP-ECC developed by Yang [3] by investigating the influences of matrix flowability, fiber mixing procedure, and curing conditions. The basic mechanisms that enhance tensile ductility of HTPP-ECC through flowability control, mixing procedure modification, and water-curing are discussed from the view point of micromechanics underlying ECC design, with supporting evidence from fiber bridging stress–crack width (σ–δ) relations.

2. Experimental studies

2.1. Materials and mixture proportions

Type I ordinary Portland cement (OPC) and class F fly ash conforming to the requirements of ASTM C150 [19] and ASTM C618 [20], respectively, were used in the ECC matrix. The specific gravities of OPC and fly ash are 3.15 and 2.45, respectively. The chemical analysis of fly ash indicates that it is mainly composed of SiO_2 (44%), Al_2O_3 (23%), Fe_2O_3 (8%), and CaO (14%), with other compounds in trace amounts. 83% by weight of fly ash is finer than 44 μm which indicates high pozzolanic reactivity with the hydration products of OPC. A polycarboxylate-based high range water reducing (HRWR) admixture was used to achieve flowability. HTPP fiber with 12 μm diameter and 10 mm length was used in all mixtures. The density, nominal tensile strength, Young's modulus, and elongation at rupture of HTPP fibers were 0.91 g/cm^3, 850 MPa, 6 GPa, and 21%, respectively.

The mixture proportion of ECC adapted from Yang [3] is presented in Table 1. The fly ash/cement ratio is 2.8. At the end of matrix mixing procedure (prior to fiber addition) a highly flowable matrix was obtained. HRWRA content was varied between mixtures in order to achieve two different matrix flowability. Flowability was indirectly measured with a modified Marsh cone flow test reported in Li [21]. The orifice diameter of Marsh cone was increased to 15 mm. The targeted flow times were 15–20 s for high flowability (HF) and 25–35 s for low flowability (LF).

2.2. Mixing procedures

Two different cement–mortar mixers with varying mixing capacities were used to observe the effects of mixing speed and bowl volume on the mix quality. The first mixer is a 1/6 hp countertop mixer with a 4.7 L bowl volume operating at three different mixing speeds (Table 2). The second mixer is a floor mixer equipped with a high torque motor (3/4 hp) and more voluminous bowl capacity (28.4 L) than the first. Three different mixing procedures were investigated. Countertop mixer was used for the first and second procedures (P1 & P2) with batch volume of 1.5 L. The floor mixer was used for the third mixing procedure (P3) with batch volume of 5 L. The mixing procedures are shown schematically in Fig. 1. Mixing sequence was similar for all procedures prior to fiber addition. After achieving the desired matrix flowability, as determined by Marsh cone flow test, fibers were gradually added and mixed for 2 min at the same rotational speed in mixing procedure P1 (Fig. 1a). In the procedure P2, an additional 1 min of mixing at the highest rotational speed was applied (Fig. 1b). However, countertop mixer overheated in this case which is an indication of inadequate motor torque for effective mixing. In procedure P3, an additional 3 min of mixing at the highest rotational speed was applied by using the floor mixer with high torque capacity without any problem (Fig. 1c), suggesting the adequacy of the floor mixer torque. After the completion of mixing sequence, the flow-spread diameters of fresh HTPP-ECCs were measured with an ASTM C 230 [22] flow-table.

2.3. Specimens preparation, curing and testing

After the completion of fresh tests, all mixtures were cast into dogbone-shaped and 50 mm cube molds moderately vibrated on a vibration table. Four dogbone-shaped specimens and three cubes were prepared for each mixture. The geometry of dogbone-shaped specimens used in this study is shown in Fig. 2, which is in accordance with the JSCE recommendations for HPFRCC specimens [23]. Specimens were demolded one day after mixing and subjected to the following curing regimes:

1. Air curing (A): Specimens stored in laboratory conditions (23 ± 3 °C, 45 ± 5% RH) for 28 days, which is the usual practice for PVA-ECC specimens.
2. Mixed curing (WA): Specimens kept in water (23 ± 3 °C) for 7 days and then stored at room temperature until the age of 28 day, at a RH of around 45 ± 5%.
3. Water curing (W): Specimens kept in water (23 ± 3 °C) for 28 days.

Uniaxial tensile tests were performed with a servo-hydraulic test system under displacement control. The rate of displacement was 0.5 mm/min, chosen to simulate a quasi-static loading condition. Two external linear variable displacement transducers (LVDT), with a gage length of approximately 100 mm, were attached to the specimen (Fig. 2). Stress–strain curves were then recorded to determine the behavior of specimens under direct tension. First crack strength is determined from the point where the stress–strain relation becomes non-linear [23]. Peak stress and the corresponding strain value are accepted as "tensile strength" and "tensile ductility", respectively. In the cases where slight stress decrease after peak stress is observed, tensile ductility

Table 1
The mixture proportions of HTPP-ECCs (kg/m^3).

Mixture code[a]	Cement (kg/m^3)	Fly ash (kg/m^3)	Water (kg/m^3)	HTPP fiber (kg/m^3)	HRWR (kg/m^3)	Target Marsh cone flow time (s)
HF	412	1150	362	18	10.7	15–20
LF					7.4	25–35

[a] HF: matrix with high flowability, LF: matrix with low flowability.

Table 2
Properties of mixers used in this study.

Mixer type	Motor torque (hp)	Mixer bowl volume (L)	Speed-1 slow (rpm)	Speed-2 medium (rpm)	Speed-3 high (rpm)
Hobart countertop mixer	1/6	4.7	60	124	255
Hobart floor mixer	3/4	28.4	54	100	183

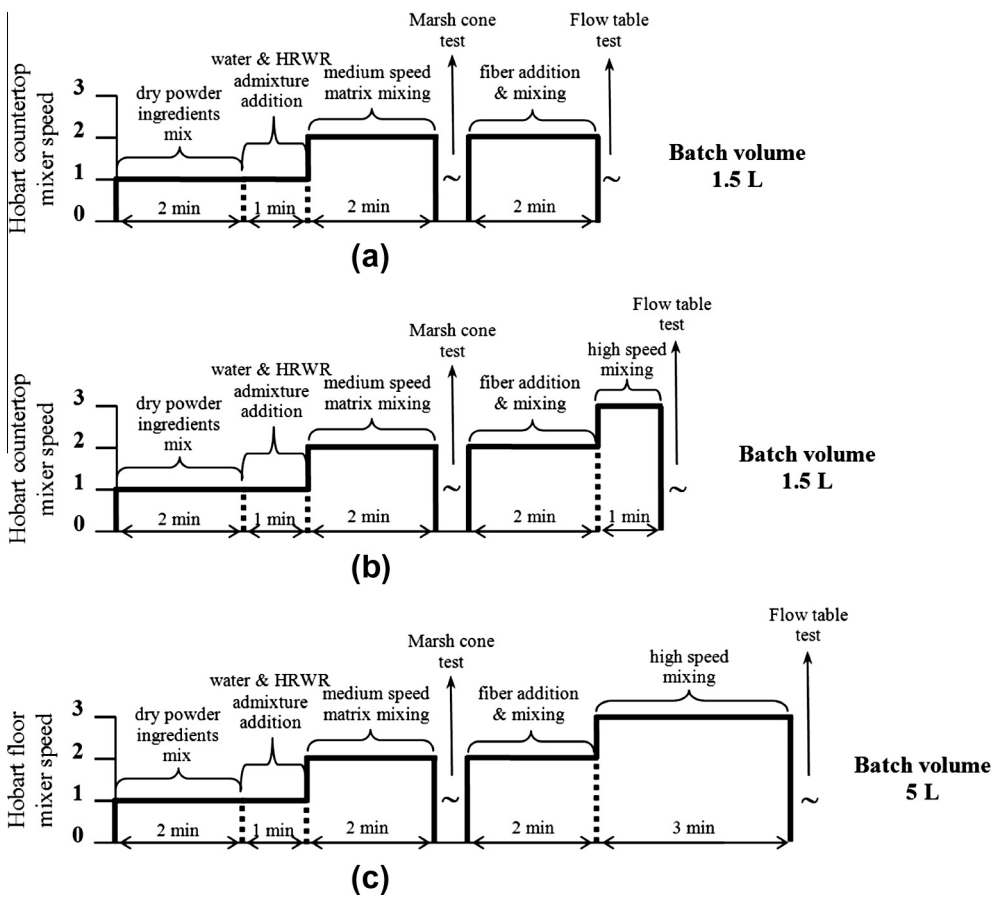

Fig. 1. Mixing sequence of procedures applied in this study: (a) P1, (b) P2, (c) P3 (see Table 2 for mixer speed in rpm).

is defined as strain at 95% of the peak stress, instead of "at peak stress". Compressive strength tests were performed at a loading rate of ~0.28 MPa/s (40 psi/s).

As multiple cracking is the indicator of tensile strain hardening capacity of ECC specimens, crack patterns were investigated in this study. A high resolution camera was used for photo documentation of damage evolution during uniaxial tensile testing. Photos were captured at the beginning of the test and at 1–2–3–4% strain values if specimen reaches these strain values. As shown in Fig. 3, the crack pattern of the focused region (gage length L – 15 mm) was used in analysis. 15 mm is the width of a holder bar in the LVDT fixture. Pixel resolution varied between 20 and 45 μm depending on the gage length (L). The number of cracks is counted with the following assumption: If a crack is visible for more than half of the specimen width, it is counted as a separate crack. Crack widths (CW) were calculated using the following formula:

$$CW(\text{mm}) = \frac{(L-15)^{*} c_{pixel}}{y_{pixel}} \quad (1)$$

where L is gage length in mm, c_{pixel} is the average crack width of each crack in pixels; y_{pixel} is the height of captured area between LVDT attachments in pixels. c_{pixel} is measured by counting the vertical pixel number of each crack image. The cracks formed out of gage length were not taken into consideration. This method is only applicable to specimens that exhibit crack widths larger than 20 μm due to resolution restraints. Crack widths smaller than 20 μm may not be detected with this method.

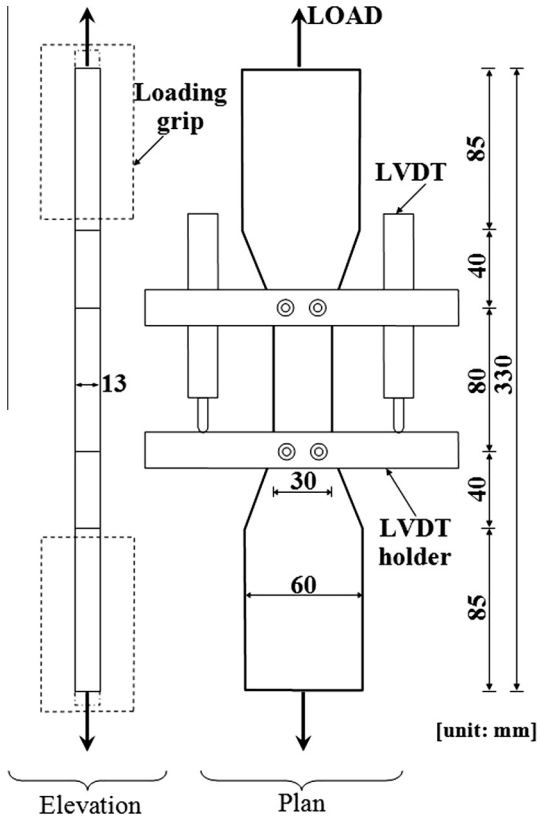

Fig. 2. Dimensions and loading configuration of dogbone-shaped specimen for uniaxial tensile testing.

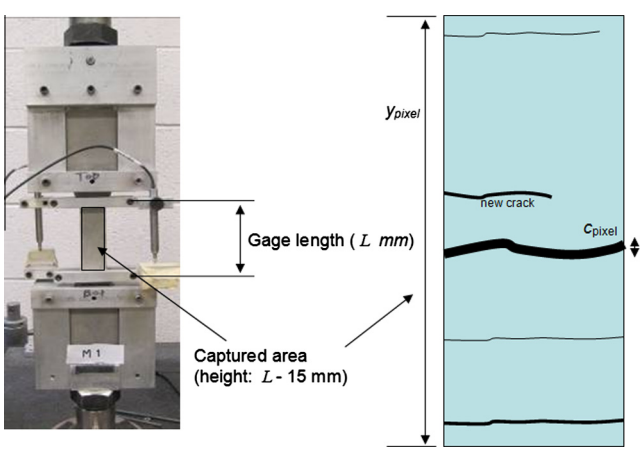

Fig. 3. Methodology of average crack width determination from crack pattern analysis.

3. Results and discussion

3.1. Fresh state tests

The spread-flow diameters of fiber reinforced HF and LF mixtures prepared with mixing procedure P1 and P2 were photographed and presented in Fig. 4. In general, spread flow diameters of fiber reinforced mixtures are proportional to the matrix flowability. This is observable in Fig. 4 as the HF mixtures show larger spread flow diameters than LF mixtures for both mixing procedures P1 and P2. Although better flowability is generally preferable for moldability and practical use, visual observations showed that HF mixtures are more susceptible to bleeding and fiber clumping. With P1 mixing procedure, significant amount of fiber clumping was observed in case of HF mixtures. The degree of fiber clumping was reduced (although not completely eliminated) in case of LF mixture, when the same mixing procedure (P1) was employed. With the application of additional 1 min of high speed mixing in procedure P2, the degree of fiber clumping was further reduced for both HF and LF mixtures. In spite of the improvements in fiber dispersion in procedure P2, the high speed mixing was not enough to fully breakdown the fiber clumps as the torque capacity of countertop mixer is limited. Thus, the proper matrix cohesion obtained in LF mixtures along with fast mixing speed seems to result in the best fiber dispersion among the above.

Due to above observations, only LF mixtures are prepared following the third mixing procedure (P3). A more homogeneous LF mixture was obtained by using a floor mixer with high torque capacity and mixing speed. A spread-flow value as high as 170 mm was recorded with a LF matrix despite its low HRWR admixture dosage (Fig. 4 P3-LF). Thus, effective mixing provided by procedure 3 enhanced the flow-diameter of LF mixture and eliminated fiber clumping with an additional advantage of HRWR admixture saving.

3.2. Uniaxial tensile performance

3.2.1. Specimens prepared with mixing procedure P1

The tensile stress–strain curves of specimens prepared with P1-HF and P1-LF mixtures subjected to mixed curing (WA) and water curing (W) are presented in Fig. 5. Due to significant fiber clumping in all mixtures produced with procedure P1, air curing (A) was not considered in this part of the study as it tends to worsen the mechanical performance compared to WA and W curing regimes (discussed below). Average crack widths (CW) along with standard deviations, and average crack number (CN) of 4 specimens at 1%, 2% and 3% strains are shown at the top of all figures (Fig. 5). In general, all specimens showed more than one crack. However, the crack density (number of cracks per unit length) is very low. The number of cracks is limited to 5 (HF) and 7 (LF) in case of mixed curing, and 6 (HF) and 12 (LF) in the case of water curing. Average crack widths at 1% strain are also large (~230 μm and ~150 μm for mixed curing) compared to typical PVA-ECC, which typically exhibits average crack widths smaller than 60 μm [3].

Test results in terms of first crack strength, ultimate tensile strength, tensile ductility and average crack width at 1% strain are shown in Table 3. First crack strength values of HF mixtures are lower than LF mixtures, which points towards the possibility of larger maximum flaw size in the HF mixtures compared to LF mixtures. The ultimate tensile strength values of HF mixtures are lower than that of LF mixtures due to non-homogenous fiber dispersion (results with fiber clumping) in HF mixtures. High matrix cohesion was found to be advantageous for improving the tensile ductility in the case of LF mixtures. For LF specimens, entrapment of air bubbles due to low flowability may possibly increase the number of flaws for crack propagation in the right size range.

Water cured specimens also performed better than the specimens with mixed curing in terms of tensile ductility. The highest average ductility value (2.64%) among this set of specimens is obtained from water cured specimens prepared with a cohesive matrix. The coefficients of variation in tensile ductility are very high for all specimens (15–53%), which can be attributed to the fiber clumping as a result of insufficient mixing (Table 3). Overall, LF mixtures with water curing had better tensile performance, particularly tensile ductility, compared to HF mixtures with mixed water–air curing.

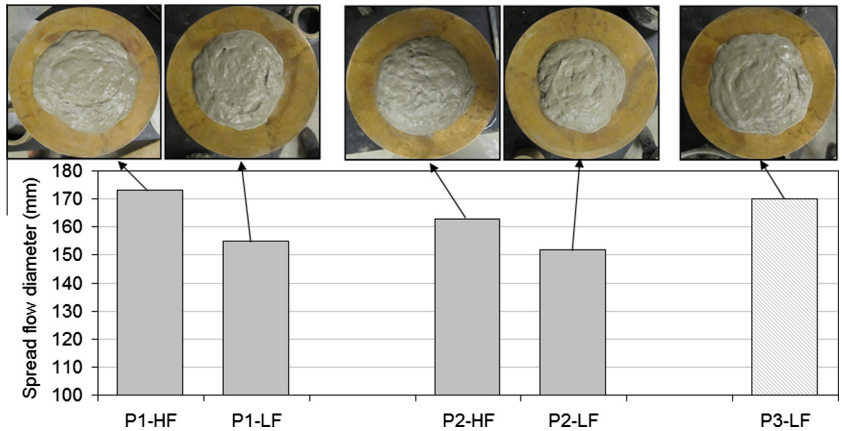

Fig. 4. The spread-flow diameters of fiber reinforced HF and LF mixtures prepared with different mixing procedures (see Fig. 1 for P1, P2 and P3 procedures).

3.2.2. Specimens prepared with mixing procedure P2

As explained above, mixing procedure P2 is essentially P1 plus additional 1 min of mixing at high speed (Fig. 1), which significantly improved the fiber dispersion in both high and low flowable mixtures. Two curing regimes, air curing (A) and water curing (W) (explained in Section 2.3), were applied to the mixtures cured with procedure P2. Similar to P1, both mixtures with high (HF) and low (LF) flowability were produced for each curing regime, resulting in a set of four mixtures.

The tensile stress–strain curves and results of crack pattern analysis for mixtures produced with procedure P2 are presented in Fig. 6. Compared to the P1 series, improvements in the ultimate tensile strength values of all P2 series specimens are observed, which indicates better fiber dispersion in P2 specimens than P1 specimens according to the principles of micromechanics. Another important difference between the tensile performances arises from different curing regimes. Water curing significantly improved the multiple cracking performances and tensile ductility of specimens compared to air-cured ones. The average number of cracks increased from 4 (Fig. 7b) to 25 (Fig. 7d), the average crack widths at 1% strain decreased from 258 to 74 μm in LF mixtures when the curing regime was changed from air to water. Similar improvements are observable in HF mixtures. Overall, additional mixing time at fast speed in P2 compared to P1 and water curing instead of air curing improved the multiple cracking performance of HTPP-ECC.

Tensile properties of HTPP-ECCs (Fig. 6) produced with procedure P2 are summarized in Table 4. Higher first crack strengths and ultimate tensile strengths (up to about 4.25 MPa for LF specimens) were recorded for the P2 series in comparison to the P1 series. From Table 4, it can be observed that curing causes no significant difference between ultimate tensile strength values of ECC. On the other hand, the average tensile ductility of water-cured specimens (1.96% and 3.23%) is significantly higher than that of air-cured specimens (0.80% and 0.81%). While high matrix cohesion (comparatively low flowability) enhanced the tensile ductility of water-cured specimens (from 1.96% to 3.23%), no such improvement was observed in the case of air-cured specimens. The beneficial effect of curing on tensile ductility can be attributed to the improved bond between HTPP fiber and matrix due to the formation of additional hydration products in the vicinity of HTPP fibers. Loss of internal curing water at low humidity in the case of air curing may interrupt the formation of hydration products at the transition zone between matrix and HTPP fibers. According to Table 4, coefficients of variation in tensile ductility are lower for specimens prepared with low flowable matrix compared to ECC with high flowable matrix. Thus, longer mixing time (at higher speed) in procedure P2 (than P1), relatively high matrix cohesion, and water curing have positive effects on the tensile performance of HTPP-ECC.

3.2.3. Specimens prepared with mixing procedure P3

Unlike the aforementioned procedures (P1 and P2), in which the batch volume was approximately 1.5 L and the mixer torque capacity was limited, a batch volume of 5 L with additional mixing time and greater torque were used in Procedure P3 (Fig. 1). In this procedure, only high cohesion matrix (low flowability) was prepared. 12 dog-bone specimens were prepared and subjected to three different curing conditions: air curing (A), mixed curing (WA) and water curing (W) (explained in Section 2.3).

The tensile stress–strain curves and crack pattern analysis of the P3 series of specimens are presented in Fig. 7. In addition to the stress–strain curves, crack pattern photograph of P3-LF-W-4 specimen at 4% strain is also shown in the same figure. In this photograph, 28 cracks are counted on this specimen with an average crack spacing of about 3 mm under 3.5 MPa tensile stress. This specimen represents the highest crack density achieved in this study. According to crack pattern analysis, average number of cracks successively increase from 7 to 13 to 23 and the average crack width at 1% strain decreases from 95 μm to 88 μm to 62 μm as the curing regime is changed from A to WA to W. In most cases, crack width variability at any given strain is also reduced with water curing. Tables 3 and 4 clearly show the decrease in coefficient of variations of crack width by water curing. These results reaffirm the conclusion from P1 and P2 series of specimens that extending the water curing stage enhances the robust multiple cracking performance of HTPP-ECC.

Tensile properties of HTPP-ECC prepared with P3 procedure are summarized in Table 5. Tensile ductility tends to increase with longer water curing; however, tensile strength remains nearly the same. Tensile strain capacity as high as 3.91% was recorded from specimens (P3-LF-W) cured in water, while average tensile strength of these specimens was 3.6 MPa. A slight decrease in ultimate tensile strength of P3 specimens compared to P2 specimens was observed, which may be attributed to air entraining effect of fibers and HRWR due to prolonged mixing. Coefficients of variation in tensile ductility of P3 specimens were equal or relatively lower than that for the specimens prepared with P2 mixing procedure (Table 5). Overall, P3 procedure enhanced the tensile performance of HTPP-ECC particularly in terms of tensile ductility and consistency of properties.

3.3. Compressive strength performance

Average compressive strength values of 50 mm cube specimens prepared with various matrix flowability, mixing procedure, and

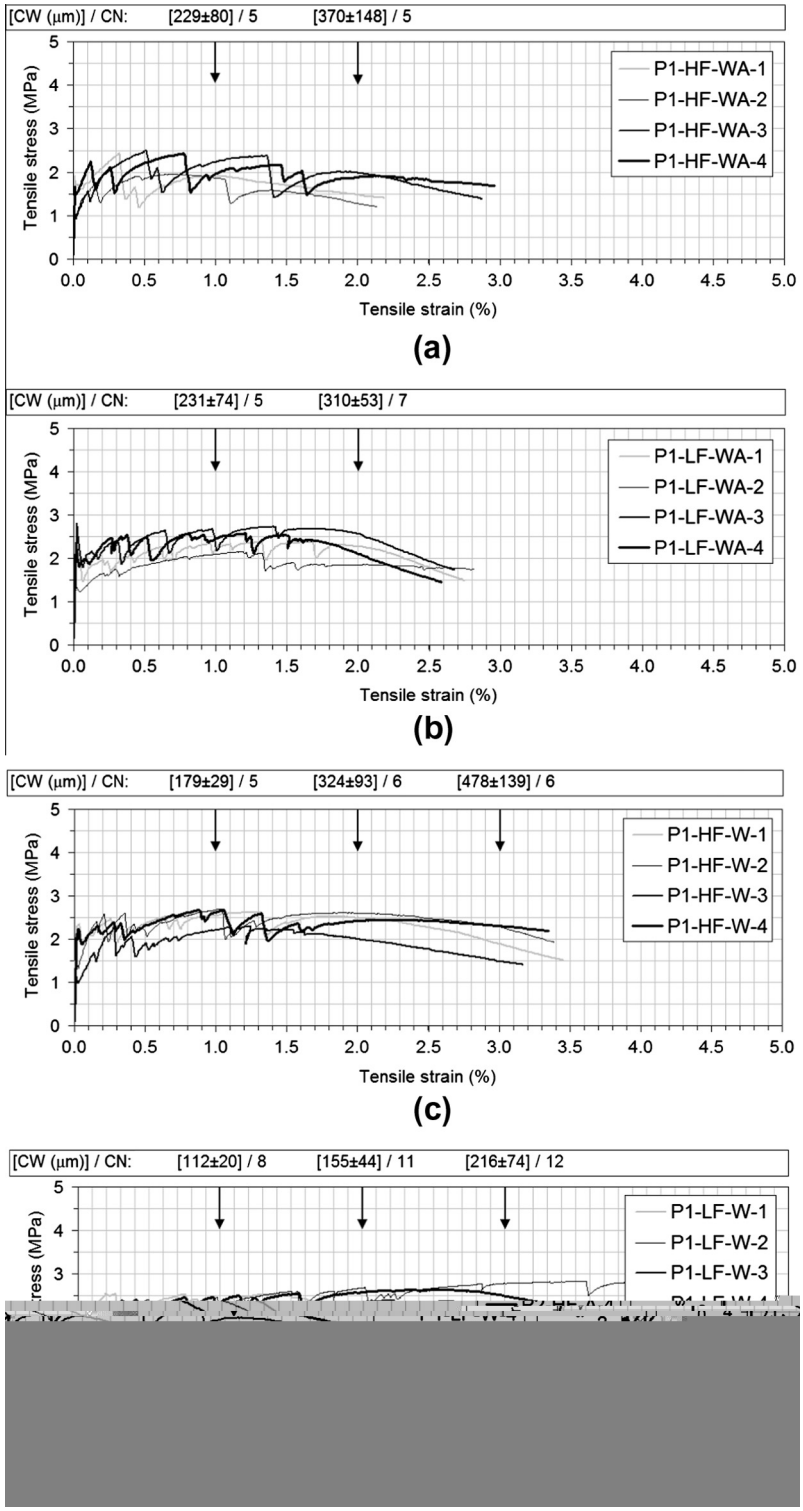

Fig. 5. Tensile stress–strain curves of specimens prepared with P1-HF and P1-LF mixtures subjected to mixed curing (WA) and water curing (W) (CW: average crack width and CN: average crack number at designated strain).

curing conditions are plotted in Fig. 8. LF mixtures showed slightly lower compressive strengths than HF mixtures (for P1 and P2 series), which is attributable to air entrainment during mixing of a relatively cohesive mixture, similar to the observations in a previous research [21] on PVA-ECC.

Among various curing conditions, the lowest compressive strength values were recorded for the specimens (P2 and P3 series) cured in air (between 30 and 40 MPa). The degree of cement hydration is limited in the absence of water curing, as the mixtures have a low water/cementitious material (w/cm) ratio of only 0.23. In addition, micro-cracking induced by drying shrinkage negatively affects the compressive strength values. It is interesting to note that, in spite of a decrease in compressive strengths of air-cured mixtures, their tensile strength was approximately similar to that

of the water-cured mixtures (Tables 3–5); however the tensile ductility of air-cured mixtures was significantly lower than that of water-cured mixtures for the reasons discussed in detail in the numerical micromechanics-based analysis proposed in Section 4.

The influence of mixing procedure on compressive strength values can be compared under constant matrix flowability and curing conditions. For instance, improvement of mixing effectiveness (from P1 to P3) successively increased the compressive strength values from about 40 MPa up to 70 MPa in case of LF-W specimens (Fig. 8). Mix homogeneity through more effective mixing and improved bond between HTPP fiber and matrix by water curing (which stabilizes the axial splitting crack) were found to be the most dominant factors influencing the compressive strengths.

4. Micromechanical modeling and application of fiber bridging model to HTPP-ECCs cured at different conditions

4.1. Basics of micromechanical modeling

According to the micromechanics based design theory of ECC two necessary conditions must be satisfied to ensure strain-hardening [24,25]. The first condition (Strength Criterion) requires that the fiber bridging capacity σ_0 should be greater than the matrix cracking strength σ_{cr} on any given crack plane. The second condition (Energy Criterion – Eq (2)) requires that the crack tip toughness J_{tip} should be less than the complementary energy J'_b of fiber bridging (Fig. 9):

$$J_{tip} \leqslant \sigma_0\delta_0 - \int_0^{\delta_0} \sigma(\delta)d\delta \equiv J'_b \tag{2}$$

Due to the random nature of preexisting flaw size and fiber distribution in ECC, a large margin between J'_b and J_{tip} is preferred for high tensile ductility. Additionally, from the view point of strength criterion a larger $\sigma_0/\sigma_{cr(fc)}$ ratio is required for saturated multiple cracking. $\sigma_{cr(fc)}$ is the cracking stress required for the initiation of the first crack in the ECC matrix. As a result, pseudo strain-hardening (PSH) performance indices (defined as $\mathrm{PSH}_{\mathrm{energy}} = \frac{J'_b}{J_{tip}}$ and $\mathrm{PSH}_{\mathrm{strength}} = \frac{\sigma_0}{\sigma_c}$) have been used to quantitatively evaluate the two margins [26,27]. Materials with larger PSH indices have better chance of saturated multiple cracking.

The $\mathrm{PSH}_{\mathrm{strength}}$ can be improved by increasing the fiber bridging capacity σ_0 through the use of a higher fiber dosage; however, it leads to higher cost, potentially poor workability, and inhomoge-

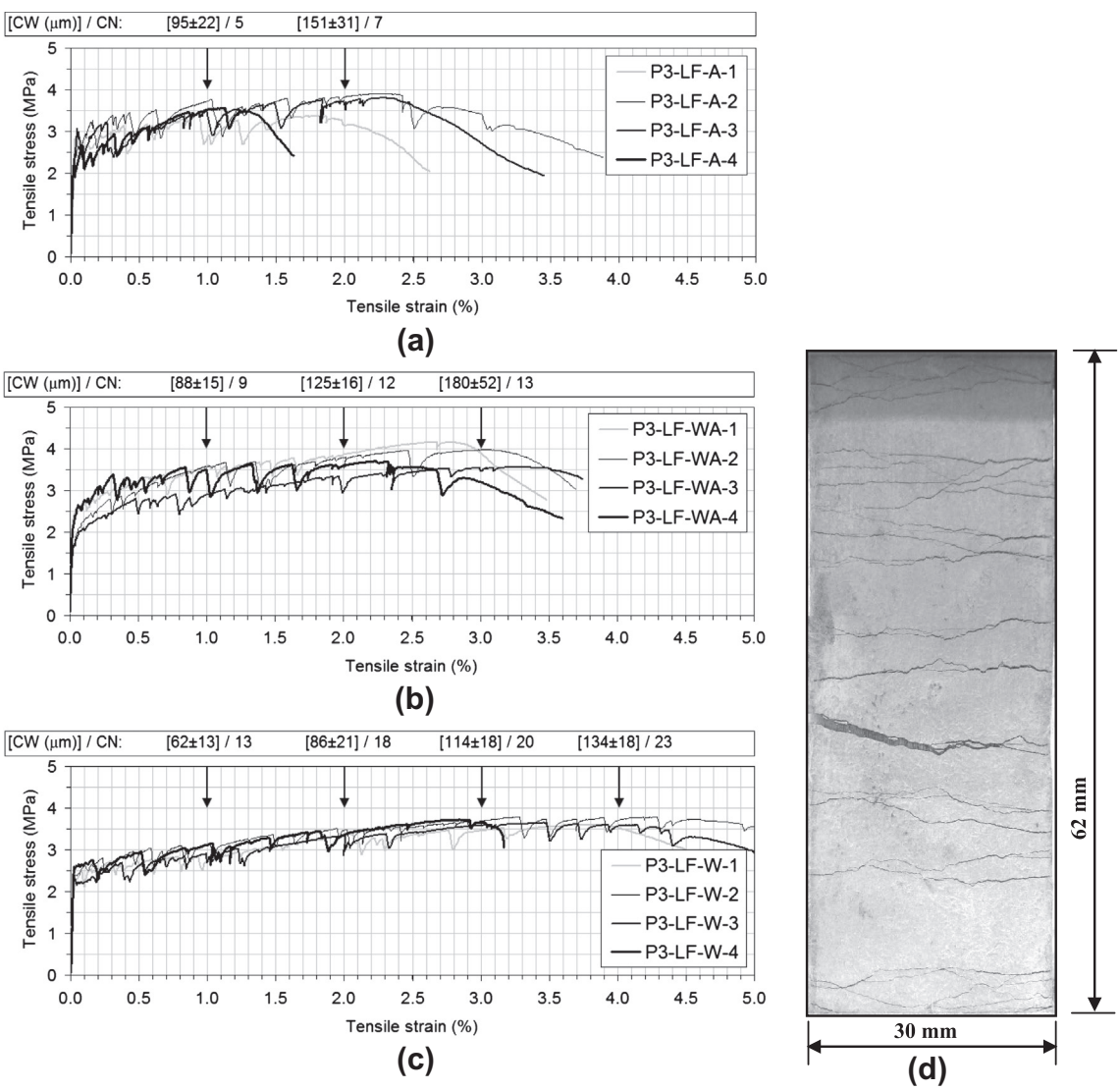

Fig. 7. Tensile stress–strain curves of specimens prepared with P3-LF mixtures subjected to (a) air curing (A), (b) mixed curing, (c) water curing (W), (d) Crack pattern of P3-LF-W-1 specimen at 4% strain.

Table 4
Tensile properties of specimens prepared with mixing procedure P2 and subjected to air curing (A) and water curing (W) conditions.

Mixture code	First crack strength (MPa)[a]	Ultimate tensile strength (MPa)[a]	Tensile ductility (%)[a]	Average crack width at 1% strain (μm)[a]
P2-HF (A)	3.26 ± 0.52 (16%)	4.05 ± 0.30 (7%)	0.81 ± 0.52 (64%)	116 ± 33 (28%)
P2-LF (A)	2.74 ± 0.58 (21%)	4.29 ± 0.33 (8%)	0.80 ± 0.31 (39%)	258 ± 146 (57%)
P2-HF (W)	1.98 ± 0.43 (22%)	3.79 ± 0.15 (4%)	1.96 ± 1.05 (53%)	95 ± 24 (25%)
P2-LF (W)	2.67 ± 0.62 (23%)	4.25 ± 0.13 (3%)	3.23 ± 0.53 (16%)	74 ± 14 (19%)

[a] Average ± standard deviation (coefficient of variation).

Table 5
Tensile properties of P3-LF specimens exposed to air, air–water and water curing.

Mixture code	First crack strength (MPa)[a]	Tensile strength (MPa)[a]	Tensile ductility (%)[a]	Average crack width at 1% strain (μm)[a]
P3-LF-A	2.37 ± 0.32 (13%)	3.64 ± 0.26 (7%)	1.91 ± 0.47 (25%)	95 ± 22 (23%)
P3-LF-WA	1.52 ± 0.49 (32%)	3.81 ± 0.30 (8%)	2.95 ± 0.35 (12%)	85 ± 15 (18%)
P3-LF-W	2.19 ± 0.24 (11%)	3.64 ± 0.07 (2%)	3.91 ± 0.67 (17%)	63 ± 13 (21%)

[a] Average ± standard deviation (coefficient of variation).

neous fiber dispersion. Using a fiber with high tensile strength can also improve σ_0 but it increases the cost of the composite. Controlling the fiber/matrix interfacial bond properties in a manner that utilizes the fibers most effectively seems to be a more appropriate solution [4].

The PSH_{energy} can be improved by decreasing J_{tip} through the reduction of matrix fracture toughness K_m or by using a larger flaw size c. However, excessive lowering of K_m or large flaw size c may lead to low compressive strength and low first crack strength under tension [4].

4.2. Application of fiber bridging model to HTPP-ECCs cured at different conditions

The fiber-bridging constitutive law $\sigma(\delta)$ describes the relationship between the bridging stress σ transferred across a crack by the fibers and the opening of this crack δ. The construction of the fiber-bridging constitutive law starts from micromechanics-based modeling a single fiber pull-out behavior against the surrounding matrix. The $\sigma(\delta)$ relationship can then be obtained by averaging the contributions from fibers with different embedment lengths and orientations across the crack plane [7,28]. This relationship relates the material microstructure (micro-scale) to the composite tensile strain hardening behavior (macro-scale). Therefore, controlling the $\sigma(\delta)$ curve through tailoring material microstructure is the key to successfully design ECC material properties in general, and tensile properties (tensile strain capacity, ultimate tensile strength, and steady-state crack width) in particular [3].

As observed in the experimental results in the previous section, different curing conditions can modify the composite mechanical behavior of HTPP-ECC which is further dependent on the fiber bridging performance ($\sigma(\delta)$). In this section, the influence of curing conditions on the $\sigma(\delta)$ relationship of HTPP-ECC is analytically investigated.

A MATLAB code using the numerical procedure for computing the $\sigma(\delta)$ relationship of ECC developed by Yang [3] was used for this micromechanics-based analysis. The micromechanical parameters used as model input for HTPP-ECCs cured at different conditions are listed in Table 6. Fiber properties; d_f, l_f, E_f and σ_f are provided by the manufacturer. Interface parameters; τ_0, G_d and β were measured by single fiber pull-out tests [29]. In that investigation, P3-LF matrix and three curing regimes (A, WA and W) were used. The coefficients of variations of τ_0 were 34%, 31% and 26%, for air, mixed and water cured specimens respectively. G_d and β values were very low compared to PVA fibers, however, they were also introduced to the model. The snubbing coefficient (f) and strength reduction factor (f') are closely related to fiber/matrix frictional bond, which is low for HTPP fibers. The values proposed by Yang [3] as $f = 0.39$ and $f' = 0.1$ are used in this study. The Cook-Gordon parameter was determined by using the assumption of $\alpha = 15.d_f$ (15×12 μm = 180 μm), which is appropriate for polypropylene fiber-reinforced concrete [30]. Matrix parameters E_m and σ_m were determined from tensile tests of dogbone shaped specimens. The initial slope of the tensile stress–strain curve of the composite was used as an approximate estimate for E_m. Matrix spalling coefficient $k = 500$ is chosen similar to that used in [3], as the observed micro-spall size was under 30 μm during the direct tension tests. These parameters were used as inputs in the micro-

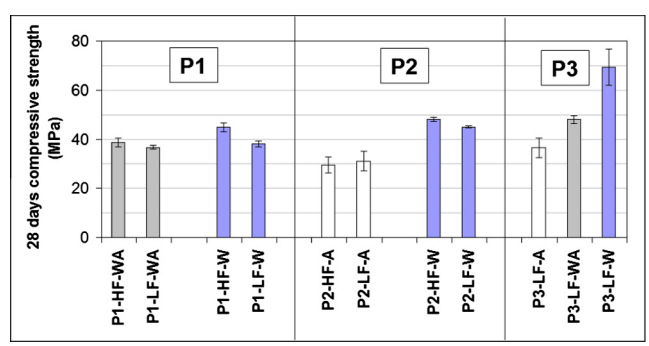

Fig. 8. Average compressive strength values of 50 mm cube specimens exposed to different curing conditions (Fig. 1 and Section 2.3 for notation details).

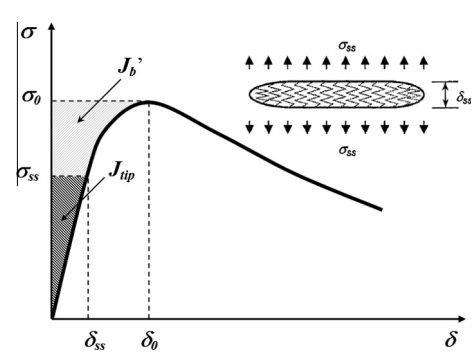

Fig. 9. Typical $\sigma(\delta)$ curve for strain-hardening material (dark shaded area represents right-hand side of Eq. (1), light hatched area represents complementary energy of composite) (adapted from Wang [2]).

Table 6
The micromechanics parameters used as model input for HTPP-ECCs cured at different conditions.

Fiber parameters									
d_f(μm)		l_f(mm)			E_f(GPa)				σ_f(MPa)
12[a]		10[a]			6[a]				850[a]
Curing condition	Interface parameters						Matrix parameters		
	τ_0(MPa)	G_d(J/m^2)	β	f	f'	α(μm)	E_m(GPa)	σ_m(MPa)	k
Air curing	0.48 [b]	0.0070 [b]	0.0043[b]	0.39[c]	0.1[c]	180[c]	12.7 [b]	1.0 ± 0.3[b]	500[c]
Mixed curing	0.99[b]	0.0051[b]	0.0020[b]				13.0[b]	1.5 ± 0.3[b]	
Water curing	1.27[b]	0.0032 [b]	0.0044 [b]				13.3[b]	2.3 ± 0.7[b]	

[a] Test results provided by manufacturer.
[b] Test result values.
[c] Assumed values.

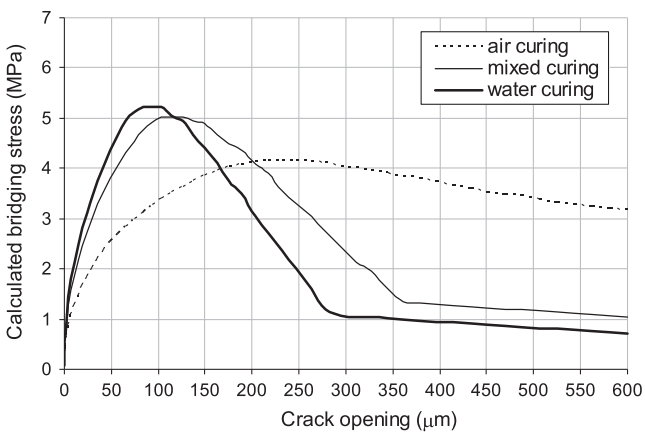

Fig. 10. Model predicted $\sigma(\delta)$ curves of HTPP-ECCs cured at different conditions.

mechanical model to determine the $\sigma(\delta)$ relation of HTPP-ECC cured under various regimes.

Relevant results of this numerical analysis consist of $\sigma(\delta)$ curves between 0-600 μm crack opening (Fig. 10), computed complementary energy of fiber bridging: J'_b (J/m^2), crack opening at bridging capacity: δ_0 (μm), and fiber bridging capacity: σ_0 (MPa) (Table 7).

According to these analytical results, σ_0 ranges between 4.1 MPa and 5.2 MPa, which is larger than the experimental ultimate tensile strength values (Table 4: P2 series: and 3.8–4.3 MPa, Table 5: P3 series: 3.6–3.8 MPa). Due to the inherent inhomogeneity of fiber dispersion in the ECC and other fiber reinforced mixtures, various specimen cross sections are bridged by different number of fibers [31,32]. As a result, the final failure occurs at the crack with least number of effective fibers. One of the conditions of multiple cracking, therefore, requires the stresses at which cracks initiate to be smaller than the maximum bridging capacity of the least bridged crack [33]. Thus, the difference between the values of σ_0 and experimental ultimate tensile strengths of HTPP-ECC may be attributed to the difference between the actual fiber distribution and the assumptions of uniform 2D distribution and a uniform fiber volume fraction of 2% used in the model.

Crack opening at bridging capacity decreased with water curing according to $\sigma(\delta)$ curves presented in Fig. 10. The main reason of this improvement can be attributed to the fiber/matrix interfacial frictional bond (τ_0). From Table 6, it can be observed that τ_0 = 0.48, 0.99 and 1.27 MPa for A, WA, and W curing regimes, respectively. In general, similar decreasing trend for crack widths was experimentally observed (Figs. 6 and 7).

In order to calculate the crack tip toughness ($J_{tip} = K_m^2/E_m$) for evaluating the PSH$_{energy}$ index for multiple cracking, matrix fracture toughnesses (K_m) of P3-LF matrices cured at different conditions were determined experimentally according to ASTM E399 [34] standard. Although this standard based on Linear Elastic Fracture Mechanics (LEFM) is proposed for metal testing, it is also applicable for testing brittle mortar matrices due to small scale yielding near the crack tip [35]. Matrix phase of P3-LF mixture without fiber was prepared by using the same procedure described in previous sections. Four beam specimens with dimensions 305 × 76 × 38 mm^3 were prepared for each curing regime. Beam specimens were notched with notch-depth to total beam height ratio of 0.60 prior to flexural loading and the span length was 254 mm. The matrix fracture toughness of air, mixed, and water cured specimens were determined equal to 0.44 ± 0.02, 0.36 ± 0.03, and 0.32 ± 0.05 MPa m$^{0.5}$ respectively, using the ASTM E399 calculations (Table 7).

PSH indices of specimens subjected to different curing conditions were calculated with the model output data and the fracture toughness test data, and the results are shown in Table 7. The computed PSH indices are plotted against observed tensile ductility in Fig. 11. Kanda [27] proposed threshold PSH index values for achieving robust strain hardening accounting for the inhomogeneity in the material. Based on experimental data, Kanda [27] proposed these practical thresholds for PVA and PP fibers: PSH$_{strength}$ = 1.45 (PVA), and 2 (PP), PSH$_{energy}$ = 3 (for both). According to Table 7 all specimens pass the PSH$_{energy}$ threshold (Table 7 – marked in bold) which means that they have the potential of multiple cracking. However, air cured specimens failed to pass the PSH

Table 7
Calculation of energy and strength criterion from model output and relevant test results.

Specimen curing condition	Model output			J_{tip}(J/m^2)	First crack strength[a] σ_{fc} (MPa)	PSH Index (energy) J'_b/J_{tip}	PSH index (strength) σ_0/σ_{fc}	Tensile ductility[a] (%)
	Fiber bridging strength: σ_0 (MPa)	Crack opening at bridging capacity: δ_0 (μm)	Fiber bridging complementary energy J'_b (J/m^2)					
Air curing	4.16	216	217	15.2	2.37	**14.3**	1.8	1.90
Mixed curing	5.00	115	145	10.0	1.52	**14.5**	**3.3**	2.95
Water curing	5.22	93	121	7.8	2.19	**15.5**	**2.4**	3.91

[a] From Table 5.

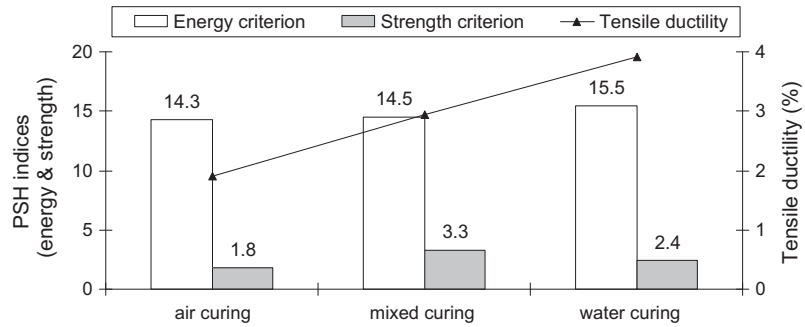

Fig. 11. Relationship between PSH indices and tensile ductility of HTPP-ECCs cured at different conditions.

strength index threshold due to their comparatively high first crack strength. Low tensile ductility of air-cured specimens from direct tension tests confirmed the applicability of these index limits.

Results of experimental and analytical studies showed that water curing, compared to air curing, increased the fiber bridging capacity and decreased the matrix toughness. The larger gap between first crack strength and ultimate strength, in the case of water curing, enables the activation of more smaller flaws within the matrix and results in an improved multiple cracking behavior and tensile ductility.

5. Conclusions

- This study showed that the processing details of ECC are as important as the selection of proper ingredients and mix proportions. Control of matrix flowability, efficient mixing, and water curing are key factors for achieving robust strain hardening and multiple cracking in HTPP-ECC.
- According to the test results, matrix cohesion should be high enough to facilitate fiber dispersion. Modified Marsh cone flow time of 25–35s is found more appropriate. Matrix with high flowability (15–20s) causes fiber clumping and resulted in poor strain hardening performance. However, cohesive matrix itself does not guarantee homogenous material production and tensile ductility, as inefficient mixing and improper curing conditions may negatively influence the performance of HTPP-ECC.
- Ultimate tensile strength and ductility values of HTPP-ECC improved in magnitude and consistency with changes in mixing procedure. Fiber clumping was significantly reduced with longer mixing time, higher mixing speed, and a mixer with higher torque.

Unlike PVA-ECC, water curing is beneficial for tensile ductility in HTPP-ECC due to the improved HTPP fiber–matrix interfacial frictional bond strength (τ_0). Micromechanical analysis showed that higher τ_0 causes an increase in fiber bridging strength (σ_0). Although the increase in τ_0 also reduces the complementary energy (J_b'), the PSH_{energy} is still high enough (due to low J_{tip}) for ensuring strain hardening.

Acknowledgements

This study was conducted at Advanced Civil Engineering – Materials Research Laboratory (ACE-MRL: http://ace-mrl.engin.umich.edu/), University of Michigan, Ann Arbor, MI. Financial support for the first author provided by TUBITAK (The Scientific and Technological Research Council of Turkey) under the Grant No. 2219 (International post-doctoral research fellowship programme) is acknowledged. The second author is grateful to YOK (The Council of Higher Education, Turkey) for the fellowship, which made it possible to conduct this research at the University of Michigan. Materials supply from Lafarge (cement), Headwaters (fly ash), WR Grace (HRWRA), and Saint-Gobain Brasil (HTPP fiber) is also gratefully acknowledged.

References

[1] Zhou J, Qian S, Ye Q, Copuroglu O, Breugel K, Li VC. Improved fiber distribution and mechanical properties of engineered cementitious composites by adjusting the mixing sequence. Cement Concr Compos 2012;34:342–8.
[2] Wang S. Micromechanics based matrix design for engineered cementitious composites. The University of Michigan, PhD Thesis (Civil Engineerin g); 2005. 222p.
[3] Yang E-H. Designing added functions in engineered cementitious composites. The University of Michigan, PhD Thesis (Civil Engineering); 2007. 276p.
[4] Li VC. Tailoring ECC for special attributes: a review. Int J Concr Struct Mater 2012;6(3):135–44.
[5] Li VC. From micromechanics to structural engineering – the design of cementitious composites for civil engineering applications. JSCE J Struct Mech Earthquake Eng 1993;10(2):37–48.
[6] Li VC. Can concrete be bendable? J Am Sci 2012;100(6):484–93. November–December.
[7] Lin Z, Li VC. Crack bridging in fiber reinforced cementitious composites with slip-hardening interfaces. J Mech Phys Solids 1997;45(5):763–87.
[8] Redon C, Li VC, Wu C, Hoshiro H, Saito T, Ogawa A. Measuring and modifying interface properties of PVA fibers in ECC matrix. ASCE J Mater Civil Eng 2001;13(6):399–406. November/December.
[9] Li VC, Wang S, Wu C. Tensile Strain-hardening Behavior of PVA-ECC. ACI Mater J 2001;98(6):483–92. November–December.
[10] Li VC, Wu C, Wang S, Ogawa A, Saito T. Interface tailoring for strain-hardening PVA-ECC. ACI Mater J 2002;99(5):463–72. September–October.
[11] Li VC. Engineered Cementitious Composites (ECC) – tailored composites through micromechanical modeling". In: Banthia N, Bentur A, Mufti A, editors. Fiber reinforced concrete: present and the future. Canadian Society of Civil Eng, Montreal; 1998. p. 64–97.
[12] Ochi T, Okubo S, Fukui K. Development of recycled PET fiber and its application as concrete-reinforcing fiber. Cement Concr Compos 2007;29:448–55.
[13] Kim SB, Yi NH, Kim HY, Kim J-HJ, Song Y-C. Material and structural performance evaluation of recycled PET fiber reinforced concrete. Cement Concr Compos 2010;32:232–40.
[14] Fraternali F, Ciancia V, Chechile R, Rizzano G, Feo L, Incarnato L. Experimental study of the thermo-mechanical properties of recycled PET fiber-reinforced concrete. Compos Struct 2011;93:2368–74.
[15] Fraternalli F, Farina I, Polzone C, Pagliuca E, Feo L. On the use of R-PET strips for the reinforcement of cement mortars. Composites: Part B 2013;46:207–10.
[16] Michels J, Waldmann D, Maas S, Zürbes A. Steel fibers as only reinforcement for flat slab construction – experimental investigation and design. Constr Build Mater 2012;26:145–55.
[17] Caggiano A, Cremona M, Faella C, Lima C, Martinelli E. Fracture behavior of concrete beams reinforced with mixed long/short steel fibers. Constr Build Mater 2012;37:832–40.
[18] Naaman AE. Engineered steel fibers with optimal properties for reinforcement of cement composites. J Adv Concr Technol 2003;1(3):241–52.
[19] ASTM C150. Standard specification for Portland cement. Annual Book of ASTM Standards, PA, USA; 2012.
[20] ASTM C618. Standard specification for coal fly ash and raw or calcined natural Pozzolan for use in concrete. Annual Book of ASTM Standards, PA, USA; 2012.
[21] Li M. Multi-scale design for durable repair of concrete structures. The University of Michigan, PhD Thesis (Civil Engineering); 2009. 425p.
[22] ASTM C230. Standard specification for flow table for use in tests of hydraulic cement. Annual Book of ASTM Standards, PA, USA; 2008.
[23] JSCE. Recommendations for design and construction of high performance fiber reinforced cement composites with multiple fine cracks (HPFRCC). Concrete

Committee, Rokugo K. (chair), Japan Society of Civil Engineers, March; 2008. 212p.
[24] Li VC, Leung CKY. Steady state and multiple cracking of short random fiber composites. ASCE J Eng Mech 1992;188(11):2246–64.
[25] Li VC. Damage tolerance of engineered cementitious composites. In: Karihaloo BL, Mai YW, Ripley MI, Ritchie RO, editors. Advances in fracture research, proc, 9th ICF conference on fracture, Sydney, Australia, Pub. Pergamon, UK, p. 619–30.
[26] Kanda T, Li VC. Practical design criteria for saturated pseudo strain hardening behavior in ECC. J Adv Concr Technol 2006;4(1):59–72.
[27] Kanda T. Design of engineered cementitious composites for ductile seismic resistant elements. PhD dissertation, department of civil and environmental engineering, University of Michigan, Ann Arbor; 1998. 329 p.
[28] Li VC, Wang Y, Backer S. A micromechanical model of tension-softening and bridging toughening of short random fiber reinforced brittle matrix composites. J Mech Phys Solids 1991;39(5):607–25.
[29] Felekoglu B. Development of cost-effective strain hardening engineered cementitious composites. Tubitak-2219: international post doctoral research fellowship programme, 2. Progress, Report; 2013. 41p.
[30] Li VC, Stang H, Krenchel H. Micromechanics of crack bridging in fiber reinforced concrete. J Mater Struct 1993;26:486–94.
[31] Caggiano A, Etse G, Martinelli E. Zero-thickness interface model formulation for failure behavior of fiber-reinforced cementitious composites. Comput Struct 2012;98–99:23–32.
[32] Tosun-Felekoğlu K, Felekoğlu B, Ranade R, Lee BY, Li VC. The role of flaw size and fiber distribution on tensile ductility of PVA-ECC. Compos B Eng 2014;56:536–45.
[33] Ranade R, Stults MD, Lee B, Li VC. Effects of fiber dispersion and flaw size distribution on the composite properties of PVA-ECC. In: Parra-Montesinos GJ, Reinhardt HW, Naaman AE, editors. Proc, sixth int'l workshop on high performance fiber reinforced cement composites (HPFRCC6), Ann Arbor, MI; 2011. p. 106–113.
[34] ASTM E399. Standard test method for plane-strain fracture toughness of metallic materials. Annual Book of ASTM Standards, PA, USA; 1997.
[35] Li VC, Mishra DK, Wu HC. Matrix design for pseudo strain-hardening fiber reinforced cementitious composites. RILEM J Mater Struct 1995;28(183):5.